First-principles investigation of metal-hydride phase stability: The Ti-H system

Qingchuan Xu and Anton Van der Ven
Department of Materials Science and Engineering, The University of Michigan, Ann Arbor, Michigan 48109, USA
(Received 9 May 2007; revised manuscript received 6 July 2007; published 29 August 2007)

Various factors that affect metal-hydride phase stability are investigated from first principles. As a particular example, we consider hydride stability in the Ti-H system, exploring the role of configurational degrees of freedom, zero-point vibrational energy as well as coherency strains. The tetragonal γ-TiH phase is predicted (within generalized gradient approximation) to be unstable relative to hcp Ti (α phase) and the fcc based δ-TiH_2. Zero-point vibrational energy significantly affects the formation energies in this system and makes the γ phase even less stable relative to hcp Ti and δ-TiH_2. The effect of stress and strain on the stability of the γ phase is also investigated showing that coherency strains between hydride precipitates and the hcp Ti matrix stabilize γ-TiH relative to α-Ti and δ-TiH_2. We also find that hydrogen prefers octahedral sites at low hydrogen concentration and tetrahedral sites at high concentration. Both harmonic vibrational as well as electronic origins for the cubic to tetragonal phase transformation of TiH_2 are investigated, and we argue that anharmonic vibrational degrees of freedom are likely to play an important role in stabilizing cubic TiH_2.

DOI: 10.1103/PhysRevB.76.064207 PACS number(s): 64.60.Cn, 64.70.Kb, 63.20.Ry, 64.60.My

I. INTRODUCTION

The tendency of a solid to form hydrides makes it a potential hydrogen storage material. This tendency also makes structural materials susceptible to hydrogen embrittlement. An understanding of the thermodynamics and kinetics of hydride formation is therefore required in the design of new hydrogen storage materials as well as alloys that are resistant to hydrogen embrittlement.

The insertion of hydrogen into a host material for storage purposes is often accompanied by phase transformations, whereby a hydride phase consumes the original host phase.[1] In a good hydrogen storage material, these phase transformations proceed reversibly and with minimal mechanical damage that may arise from differences in volume between the various phases participating in the transformation.

Hydrogen embrittlement has several origins depending on environmental and loading conditions. These include (i) the formation of brittle hydrides,[2–4] (ii) a hydrogen induced reduction in cohesive strength of the solid,[5–8] and (iii) hydrogen enhanced local plasticity (HELP) whereby the presence of hydrogen atoms enhances dislocation glide.[9–11] In a particular alloy, all three mechanisms may play a role, with hydride formation followed by hydride cleavage typically dominating under slow loading rates and the HELP mechanism dominating at high strain rates.[3] The change in mechanism with loading rate arises from kinetic factors that prevent the rapid formation of brittle hydride phases as the solid is strained.

A first step in understanding hydride formation in hydrogen storage materials or during mechanical loading in structural materials is the determination of hydride phase stability. Often, hydrides are compounds in which hydrogen orders over interstitial sites of the host material. Not all hydrides are stoichiometric, though, and can exhibit considerable configurational disorder. Since hydrogen is the lightest element, zero-point vibrational energy is potentially also important in determining hydride phase stability. Finally, hydrides often form in the solid state, where coherency strains and internal stresses may alter relative stabilities of various hydride phases.

In this paper, we investigate different factors that determine hydride phase stability from first principles. We focus on hydride formation in Ti, an important structural material that is well known to be susceptible to hydrogen embrittlement.[3,12–14] While Ti in and of itself is currently not considered a viable hydrogen storage material, the thermodynamic and kinetic principles that dominate hydride formation in this metal are similar to those occurring in well-known hydrogen storage materials such as Ni-based alloys (with rare-earth elements[15] or with transition metal ions[16]). Furthermore, Ti can serve as an alloying element in Ni- and Fe-based metal-hydride storage materials,[17,18] while the addition of $TiCl_3$ to $NaAlH_4$, a promising hydrogen storage material, has been shown to significantly enhance its hydrogen (de)sorption reactions.[19]

The hydrides that form in Ti are crystallographically identical to those that form in Zr,[20,21] an important component in nuclear fuel rod cladding. In pure α-Ti (hcp), three hydride phases can form:[22–25] (i) δ-TiH_{2-z} (where z ranges between 0 and 0.5), (ii) ε-TiH_2, which is a tetragonally distorted form of δ, and (iii) γ-TiH. We explore the role of configurational degrees of freedom, vibrational degrees of freedom, and coherency strains in affecting hydride phase stability with a particular focus on the relative stability of γ-TiH, as this hydride is believed to be metastable but is nevertheless observed experimentally in the form of coherent precipitates.[23–25] We also explore the nature of the cubic to tetragonal phase transformation of TiH_2 that occurs around room temperature.[22]

II. METHODS

A prediction of phase stability requires a comparison of free energies of different phases at finite temperature. The free energy G of a system is formally related to the partition function

$$Z = \sum_s \exp\left(-\frac{E_s}{k_B T}\right) \quad (1)$$

according to $G=-k_BT\ln Z$, where k_B is the Boltzmann constant and T is the absolute temperature. The sum in Eq. (1) extends over all excited states s of the solid, each having energy E_s. For metal phases and their hydrides, the states s include configurational, vibrational, and electronic excitations. [First-principles energies are usually calculated at zero pressure P, and the PV_s term that should appear in the exponential of Eq. (1), where V_s is the volume of excited state s, can then be ignored.] Configurational degrees of freedom arise from all the possible ways of distributing hydrogen over the interstitial sites of the metal host. Often, vibrational and electronic excitations are neglected in first-principles investigations of phase stability in multicomponent solids;[26–34] however, due to the low mass of hydrogen atoms, zero-point vibrational energy can be important.[35] The excitation energies E_s should be calculated from first principles (e.g., with density functional theory), but since the number of excitations is astronomically large, it is necessary to resort to a model that extrapolates first-principles energies.

By assigning an occupation variable σ_i to each interstitial hydrogen site i within the host, which is +1 if the site is occupied and −1 if it is vacant, it is possible to uniquely specify a particular hydrogen-vacancy configuration with the collection of occupation variables $\vec{\sigma}=\{\sigma_i\}$. Sanchez *et al.*[36] showed that any property that depends on configuration can be expanded in terms of polynomials of the discrete occupation variables σ_i. The dependence of the (fully relaxed) energy on configuration, for example, then takes the form

$$E(\vec{\sigma}) = V_o + \sum_i V_i\sigma_i + \sum_{i,j} V_{ij}\sigma_i\sigma_j + \sum_{i,j,k} V_{ijk}\sigma_i\sigma_j\sigma_k + \cdots, \quad (2)$$

where the indices $i,j,k,\ldots$, correspond to a collection of interstitial sites that form a cluster such as a pair cluster, a triplet cluster, etc. The coefficients V_o, V_{ij}, and V_{ijk} are called effective cluster interactions (ECI) and are constants. Equation (2), often referred to as a cluster expansion, extends over all possible clusters of sites. From a practical point of view, however, it must be truncated after some maximal sized cluster.

The simultaneous treatment of configurational and vibrational degrees of freedom is possible with a coarse graining procedure,[37,38] where instead of cluster expanding the fully relaxed configurational energy $E(\vec{\sigma})$, a coarse-grained free energy $G(\vec{\sigma},T)$ is cluster expanded. $G(\vec{\sigma},T)$ accounts for vibrational and possibly electronic excitations but is constrained to a fixed hydrogen-vacancy configuration $\vec{\sigma}$. Neglecting electronic excitations, $G(\vec{\sigma},T)$ can be calculated within the quasiharmonic approximation using first-principles phonon densities of states for the solid having a configuration $\vec{\sigma}$.[38] Phonon densities of states are accessible from first principles either with a linear response method[39] or a frozen phonon approach in which force constants are extracted from calculations of restoring forces on perturbed atoms within supercells.[38,40] The vibrational free energy at fixed volume V is related, within the harmonic approximation, to the vibrational density of states $g(\nu,\vec{\sigma},V)$ according to[38]

$$F_{vib}(\vec{\sigma},T,V) = k_BT\int \ln\left[2\sinh\left(\frac{h\upsilon}{2k_BT}\right)\right] g(\upsilon,\vec{\sigma},V)d\upsilon, \quad (3)$$

where ν is a vibrational frequency. Within the quasiharmonic approximation, the coarse-grained free energy $G(\vec{\sigma},T)$ is set equal to the minimum of $E(\vec{\sigma},V)+F_{vib}(\vec{\sigma},T,V)$ with respect to V (i.e., the pressure is assumed to be zero). The ability to perform this coarse graining procedure, however, rests on the assumption that each arrangement of atoms is mechanically stable and exhibits minimal anharmonicity with respect to vibrational degrees of freedom. It will emerge that fcc based TiH_{2-z} exhibits important anharmonicity with respect to homogeneous tetragonal strain, indicating that a standard coarse graining scheme may not be sufficient to capture all relevant degrees of freedom in this system. We will argue that additional thermal excitations involving local strain fluctuations are likely to also contribute to the thermodynamic properties of TiH_{2-z}.

The ECI of a cluster expansion of either the configurational energy $E(\vec{\sigma})$ or a coarse-grained free energy $G(\vec{\sigma},T)$ need be determined from first principles. This then enables the calculation of thermodynamic properties with, for example, Monte Carlo simulations. Several techniques have been used to determine ECI from first principles, and most are based on a least squares fit of a truncated cluster expansion to the first-principles energies of different configurations.[26,41] The ECI obtained with this approach depends both on the truncation of Eq. (2) and on the selection of configurations used in the fit.

The cross-validation (CV) score is a useful criterion in selecting an optimal set of clusters.[29] The CV score is a measure of the ability of the cluster expansion to predict energies not included in the fit. There are different definitions of the CV score: the leave-one-out CV (LOO-CV) and the leave many out in which Monte Carlo sampling is used. In this work, we use the Monte Carlo CV (MCCV).[42,43] Suppose the energies of n configurations have been calculated from first principles. The algorithm involves the random removal of n_v configurations from the sample followed by a fit of the ECI to the remaining n_c structures. This procedure is repeated b times. The definition of the MCCV score is

$$(\mathrm{MCCV})^2 = \frac{1}{n_v b}\sum_{\vec{\sigma}}^{nc} [\hat{E}(\vec{\sigma}) - E(\vec{\sigma})]^2, \quad (4)$$

where $E(\vec{\sigma})$ is the calculated first-principles energy of a structure having a configuration $\vec{\sigma}$, and $\hat{E}(\vec{\sigma})$ is the cluster expansion predicted energy of $\vec{\sigma}$. Since it is impossible to enumerate all possible combinations of clusters, we search for an optimal set by using a genetic algorithm.[44] The algorithm implemented in this work uses slightly different criteria to pick clusters than that of Hart *et al.*:[44] pairs are chosen in the order of their length while only triplet, quadruplet, and larger clusters are chosen if their largest intersite distance is

less than the largest pair already included in the expansion. Once the optimal set of clusters is obtained, we use the energies of all n structures to obtain the values for the optimal ECI. The resultant ECI can then be implemented in Monte Carlo simulations to calculate finite temperature free energies.

While equilibrium at constant temperature, pressure, and concentration is determined by the minimum of the Gibbs free energy, a different characteristic thermodynamic potential must be minimized to determine phase equilibrium if the system is subjected to an anisotropic state of stress resulting from an external load or from internal coherency strains. In its most general form, a particular state of stress can be represented with a stress tensor. For simplicity and for the purpose of revealing general trends, we consider only uniaxial stress states represented by the scalar σ. Other external thermodynamic boundary conditions that are often imposed on a stressed metal susceptible to hydride formation are a constant temperature T and a constant hydrogen chemical potential μ_H, which can be controlled experimentally by fixing the hydrogen partial pressure of the environment. At fixed T, μ_H, and σ, the characteristic thermodynamic potential to be minimized to determine phase equilibrium takes the form

$$\Phi = E - TS - \mu_H N_H - V_o \sigma \varepsilon, \tag{5}$$

where E is the internal energy, S the entropy, N_H the number of hydrogen atoms, ε the strain, and V_o a reference volume of the solid with respect to which the strain is measured. When the above quantities are normalized per Ti atom, then N_H becomes 0 for pure Ti, 1 for TiH, and 2 for TiH_2. The thermodynamically stable phase at a particular T, μ_H, and σ will have the lowest value for Φ among all the phases competing for stability.

III. RESULTS

A simultaneous treatment of configurational degrees of freedom and vibrational excitations is computationally very demanding as it would require the first-principles calculation of phonon densities of states of many different hydrogen-vacancy configurations over the interstitial sites of Ti to determine the coarse-grained free energies $G(\vec{\sigma}, T)$ for each configuration. Furthermore, as will be illustrated, the Ti-H system exhibits strong anharmonicity with respect to homogeneous strain, indicating that long-wavelength strain fluctuations may contribute to the thermodynamic properties of this system. Such excitations cannot be accounted for with the coarse graining scheme[37] described above, which treats vibrational excitations within the quasiharmonic approximation. We therefore investigate configurational and vibrational degrees of freedom independent of each other to derive qualitative insight about the importance of configurational entropy, zero-point vibrational energy, and coherency strain on the stability of γ-TiH relative to hcp Ti and TiH_2.

A. Configurational degrees of freedom

1. Formation energies and relative stability of host structures

An investigation of phase stability in the Ti-H system must start with a consideration of the likely host structures that can accommodate hydrogen insertion. In this work, we focused on the hcp and fcc-Ti hosts. While bcc Ti is observed at high temperature, it is predicted to be mechanically unstable from first principles,[36] raising fundamental questions about the true nature of this high-temperature phase. Within the hcp and fcc hosts, hydrogen can reside in either octahedral or tetrahedral sites. For each Ti atom in the hcp and fcc structures, there are two four-coordinated tetrahedral sites and one six-coordinated octahedral site.

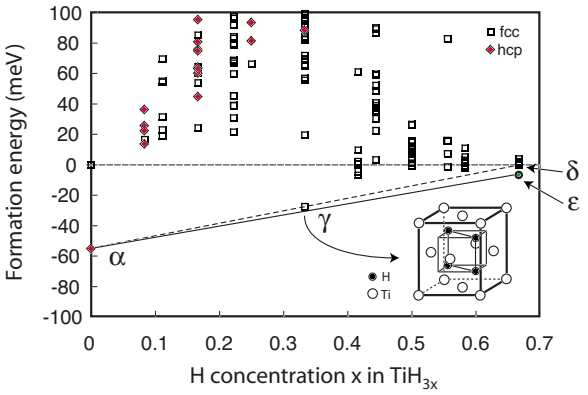

FIG. 1. (Color online) Formation energies of TiH_{3x} for fcc and hcp based hydrogen-vacancy configurations with respect to fcc Ti and δ-TiH_2.

We calculated the energy of a variety of different hydrogen-vacancy configurations over the interstitial sites of both hcp Ti and fcc Ti using density functional theory within the generalized gradient approximation (Perdew-Burke-Ernzerhof parametrization of the exchange correlation potential) as implemented in the VASP plane-wave pseudopotential code.[45,46] The core-electron interactions were treated with the projector augmented wave method,[47,48] and a plane-wave basis set cutoff energy of 400 eV was used. The k-point grids were sampled with the Monkhorst-Pack method,[49] and the partial occupancy at the Fermi level was treated with the method of Methfessel and Paxton.[50] The ionic positions and the lattice parameters of each structure were fully relaxed. Convergence tests of the energy with respect to k-point grids indicated that k-point sampling errors are less than 5 meV per TiH_{3x} formula unit.

Formation energies of the low energy configurations are illustrated in Fig. 1 in which fcc Ti and δ-TiH_2 (all tetrahedral sites filled with hydrogen) are used as reference states. For pure Ti, we find that hcp Ti is more stable than fcc Ti by 55 meV/atom and more stable than bcc by 109 meV/atom. This result is consistent with the experimental observation that hcp α-Ti is observed at room temperature. Hydrogen insertion, though, leads to a stabilization of fcc relative to hcp. At the stoichiometric TiH_2 composition, the lowest energy configuration is one in which hydrogen fills all tetrahedral sites (a CaF_2 structure). This structure corresponds to the experimentally observed δ-TiH_2. This cubic TiH_2 structure can further lower its energy by 6 meV per Ti through a tetragonal distortion, which corresponds to the experimentally observed low-temperature ε-TiH_2 phase. At intermediate concentration, an ordered phase with composition TiH is energetically favored relative to fcc Ti and δ-TiH_2, however,

TABLE I. Comparison of calculated lattice parameters with experimental results.

	a (Å)	c (Å)
hcp Ti	2.944	4.644
	2.95	4.68[a]
γ-TiH	4.1681	4.584
	4.21	4.6[b]
δ-TiH_2	4.414	
	4.404[c]	

[a]Reference 51.
[b]Reference 23.
[c]Reference 25.

not stable enough to make it a ground state relative to hcp α-Ti and δ-TiH_2 (i.e., its energy is above the dashed line in Fig. 1) or hcp α-Ti and ε-TiH_2 (i.e., its energy is above the solid line in Fig. 1). In this low energy TiH phase, the H atoms occupy half the tetrahedral sites as illustrated in Fig. 1. This H ordering is the same as that reported for the γ-TiH phase observed experimentally but believed to be metastable.[23] The particular H ordering within γ-TiH leads to a face center tetragonal unit cell with a calculated c/a ratio of 1.1. The experimental c/a ratio is 1.093.[23] A summary of calculated lattice parameters for several phases is presented in Table I. The consistency with experiment is satisfactory.[23,25,51]

Several TiH_{3x} structures with compositions close to stoichiometric TiH_2 exhibit peculiar mechanical instabilities and a strong degree of anharmonicity with respect to homogeneous strains. The energy of TiH_2 as a function of the c/a ratio, for example, is illustrated in Fig. 2(a). The energy curve displays two local minima, one with $c/a>1$ and the other with $c/a<1$. The minimum at $c/a<1$ has the lowest energy and corresponds to the ε phase observed experimentally below room temperature.[22] The difference in energy between cubic TiH_2 and tetragonal TiH_2 is predicted within the generalized gradient approximation (GGA) to be $\sim$6 meV per Ti atom. Surprisingly, the cubic form of TiH_2 ($c/a=1$), which appears experimentally above $\sim$300 K,[22] is predicted to be mechanically unstable at 0 K. Similar curves were predicted by Wolf and Herzig for TiH_2 and ZrH_2 (Ref. 52) and by Ackland for ZrH_2.[53] The calculations of Wolf and Herzig,[52] performed with FLAPW using local-density approximation (LDA) with the Hedin and Lundqvist parametrization, however, predicted the tetragonal variant with $c/a>1$ to be more stable than the $c/a<1$ variant. The discrepancy between their results and those predicted here can likely be attributed to a difference in the parametrization of the exchange correlation potential. Indeed, we recalculated the energy versus c/a with a variety of k-point meshes ranging from $8\times8\times8$ to $24\times24\times24$ for the nonprimitive cubic TiH_2 unit cell to rule out errors due to poor k-point sampling. For all k-point meshes, the $c/a<1$ tetragonal variant has the lowest energy. We also found that LDA based on the Perdew-Zunger parametrization of the exchange correlation predicts

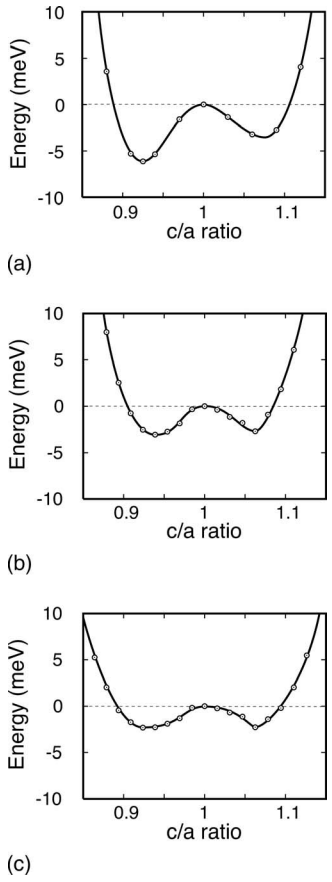

FIG. 2. Variation of the energy of TiH_{2-z} with c/a ratio (at constant volume) for (a) TiH_2, (b) $TiH_{1.75}$, and (c) $TiH_{1.5}$. A c/a ratio equal to 1 corresponds to the cubic phase.

the tetragonal variant with $c/a<1$ to have the lowest energy.

Similar mechanical instabilities with respect to a homogeneous tetragonal distortion were found for other H-vacancy configurations in fcc Ti with compositions close to TiH_2. Figures 2(b) and 2(c) illustrate the energy for two off-stoichiometric compounds as a function of the c/a ratio. The difference between the mechanically unstable cubic form and a stable tetragonal variant as hydrogen vacancies are added to TiH_2 was always found to be less than 3 meV per Ti. The mechanical instabilities of hydrogen-rich cubic TiH_{2-z} configurations complicate a rigorous description of the finite temperature excitations that determine the thermodynamic properties of this system. The strong anharmonicity with respect to homogeneous strain indicates that long-wavelength strain fluctuations are easily excited, thereby contributing to finite temperature free energies that determine phase stability. Such excitations were not explicitly investigated in this work.

2. *Cluster expansion and statistical mechanics for the fcc and hcp hosts*

The formation energies in Fig. 1 show that the hcp Ti host rapidly becomes unstable relative to the fcc-Ti host as hydrogen is inserted. This indicates that the hydrogen solubility within α-Ti (hcp) will be dilute and that the relevant thermo-

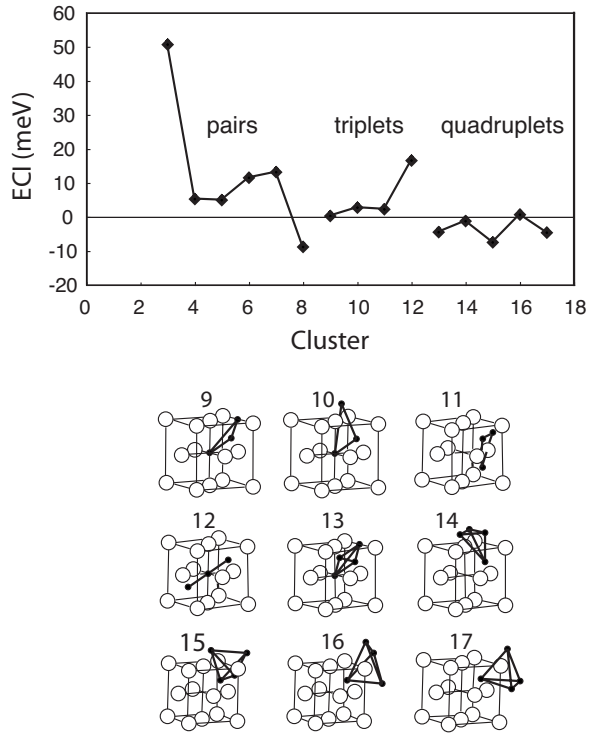

FIG. 3. Effective cluster interactions for the cluster expansion of the hydrogen-vacancy configurational energy over the interstitial sites of fcc Ti. The clusters include an empty and two point clusters (not shown), six pairs, four triplets, and five quadruplets.

dynamic properties of this phase can be treated with an ideal solution model in which interactions between different hydrogen atoms are neglected. For fcc Ti, however, nondilute hydrogen interactions are important and a cluster expansion is necessary to parametrize the formation energies for the different hydrogen-vacancy configurations in this host.

A cluster expansion for the fcc host structure was constructed by fitting Eq. (2) to formation energies of 65 different H-vacancy configurations within the fcc host with the largest supercell containing four TiH_{3x}. By minimizing the MCCV using a genetic algorithm, an optimal set of clusters was selected from a total of 79 candidates. The set includes one empty cluster, two points (for the tetrahedral and octahedral sites), six pairs, four triplets, and five quadruplets, and the values of their ECI are illustrated in Fig. 3. The root-mean-square error with respect to the structures used in the fit is 8 meV per TiH_{3x} formula unit and the leave-one-out CV (LOO-CV) is 16 meV per TiH_{3x} formula unit. The cluster expansion correctly predicts γ-TiH and δ-TiH_2 to be ground states when considering only hydrogen-vacancy configurations over the interstitial sites of fcc Ti.

It should be noted that the use of a cluster expansion for the cubic fcc based TiH_{3x} is not strictly rigorous, as this phase is mechanically unstable with respect to a tetragonal distortion for hydrogen compositions close TiH_2 (see Fig. 2 and Sec. III A 1). However, as noted above, the difference in energy between the cubic phase and the mechanically stable tetragonal variants in TiH_{2-z} was found to be less than 3 meV per Ti, except for TiH_2, for which the difference is 6 meV per Ti. As these differences in energy are very small and are of the order of typical numerical errors due to k-point sampling, we believe that the cluster expansion of Fig. 3 should provide a sufficiently accurate description of the configurational energy of cubic TiH_{2-z} observed experimentally above 300 K.[22]

In the parametrization of the cluster expansion for fcc TiH_{3x}, we used fully relaxed energies for each of the 65 H-vacancy configurations. The relaxed energies were determined with an automated relaxation procedure (i.e., conjugate gradient method within VASP). We point out, though, that this approach is not always guaranteed to find the lowest energy (mechanically stable) distortion due to symmetry constraints of the prerelaxed structure. In this work, for example, we relaxed each configuration starting with a cubic Ti-fcc host. If the H-vacancy arrangement preserves this symmetry, the relaxed structure will also be cubic and will not spontaneously relax to a mechanically stable tetragonal variant. The H-vacancy configurations that do not preserve cubic symmetry will spontaneously distort; however, the relaxed distortion may not correspond to the lowest energy tetragonal variant for that configuration. An analysis of the vibrational degrees of freedom (Sec. III B) of a subset of the 65 relaxed H-vacancy configurations used in the fit of the cluster expansion showed that several of these configurations are mechanically unstable with respect to a tetragonal distortion. The use of relaxed input energies that do not always correspond to the lowest energy distortion can contaminate the fit of a cluster expansion, leading to a reduction in its ability to predict the energies of configurations not included in the fit. However, since the difference between stable tetragonal distortions and cubic TiH_{2-z} ranges between 3 and 6 meV per Ti, we expect only a marginal increase in accuracy if a more consistent set of input energies was used in the fit of the cluster expansion (obtained, e.g., by manual relaxation of each of the 65 configurations to find the lowest energy distortion).

The cluster expansion of the H-vacancy configurational energy in fcc Ti was implemented in Monte Carlo simulations in the grand canonical ensemble. A Monte Carlo cell containing 512 unit cells (1536 interstitial sites as there are two tetrahedral sites and one octahedral site per unit cell) was used. At each temperature and chemical potential, 1000 Monte Carlo passes per site were performed after which averaging occurred over 2000 Monte Carlo passes. The relative stability between fcc and hcp hosts as a function of hydrogen concentration can be determined by a comparison of their free energies. For the fcc host, the free energies were calculated by integrating the chemical potential obtained from Monte Carlo simulations, starting from reference states where the free energy is known (e.g., at $x=0$ in TiH_{3x} for which the configurational entropy is zero,[30] or in ordered phases at low temperature where the free energy can be calculated with a low-temperature expansion[54]).

Due to the low hydrogen solubility in hcp Ti, we can accurately describe the free energy of α-TiH_{3x} with an ideal solution model (in which interactions among hydrogen atoms are neglected). The change in energy upon adding an isolated hydrogen to either a tetrahedral or octahedral site in hcp Ti was calculated in a 36-atom supercell (comparisons with

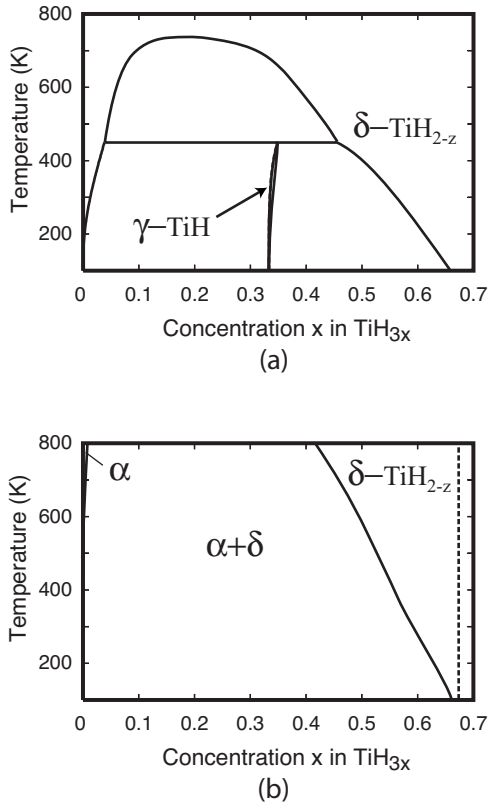

FIG. 4. Calculated phase diagrams of TiH_{3x}: (a) considering relative stability over the fcc-Ti host only and (b) considering relative stability over both the hcp and fcc hosts.

similar calculations in a 96-atom supercell showed that the 36-atom supercell is sufficiently large to approximate the dilute limit). The ideal solution free energy for interstitial occupancy in hcp Ti has one internal degree of freedom at fixed hydrogen concentration with respect to octahedral versus tetrahedral site occupancy. The relative hydrogen occupancy between octahedral and tetrahedral sites as a function of T and hydrogen concentration was determined by minimizing the ideal solution free energy with respect to this internal degree of freedom.

3. Phase diagram

Two calculated phase diagrams are illustrated in Fig. 4. Figure 4(a) shows a metastable phase diagram of TiH_{3x} over the fcc host only. Figure 4(b) shows the phase diagram of TiH_{3x} calculated by comparing free energies over both the fcc and hcp hosts, with the vertical dashed line representing the stoichiometric TiH_2 composition. Considering only the fcc host structure, Fig. 4(a) shows that two hydrides are stable: the γ hydride (TiH) and the δ hydride (TiH_2). The γ hydride is predicted to be stable only at low temperature, decomposing through a peritectoid reaction at around 450 K. This γ hydride corresponds to the face centered tetragonal TiH phase observed experimentally.[23] The δ-TiH_2 hydride, in which H occupies the tetrahedral interstitial sites of the fcc-Ti host, can tolerate a large degree of off stoichiometry, accommodated by H vacancies.

When considering relative stability over both the fcc and hcp host structures (below ~700 K), as illustrated in Fig. 4(b), only the δ-TiH_2 hydride remains stable. A large two-phase coexistence region exists between δ-TiH_2 and α-hcp-Ti, with the latter being characterized by a very dilute H solubility limit. Not included in the calculated phase diagrams is the cubic to tetragonal transition that occurs upon cooling TiH_2 to low temperatures. This transition will be discussed in Sec. III C.

Experiments by Numakura and Koiwa[23] demonstrated the existence of γ-TiH precipitates within the α phase matrix in a Ti-3 at. % H specimen. The calculated phase diagram, however, predicts that γ-TiH is metastable with respect to α-Ti and δ-TiH_2. Figure 1 shows that the formation energy of γ-TiH lies above the common tangent to the formation energies of α-hcp-Ti and δ-TiH_2. The Monte Carlo simulations show that the degree with which γ-TiH is unstable relative to α-hcp-Ti and δ-TiH_2 increases substantially with temperature. As the temperature is increased, the free energy of δ-TiH_2 decreases more rapidly than that of γ-TiH as a result of the additional configurational entropy arising from vacancy disorder in off-stoichiometric δ-TiH_{2-z}. This is clearly illustrated by the calculated free energy curves of the α, δ, and γ phases as a function of H concentration at various temperatures (Fig. 5). While the free energy of γ at low temperature lies below the common tangent to *fcc* Ti and δ-TiH_2, it is well above the common tangent to the free energies of α-hcp-Ti and δ-TiH_2. Above 450 K [the peritectoid temperature in Fig. 4(a)], the γ-TiH phase disappears altogether. These results show that when considering only configurational degrees of freedom, the γ-TiH hydride is predicted (within the first-principles GGA approach) to be unstable at finite temperature. Other factors, including vibrational degrees of freedom or coherency strain, may alter the stability of γ-TiH relative to α-hcp-Ti and δ-TiH_2 and thus show that the observation of γ-TiH by Numakura and Koiwa[23] is thermodynamically driven and not due to kinetic factors. This will be explored in subsequent sections.

4. Site occupancy

Both the fcc and hcp hosts offer tetrahedral and octahedral interstitial sites for H occupancy. The first-principles GGA calculations of formation energies of the different H-vacancy arrangements over the interstitial sites of fcc and hcp show that the preference for tetrahedral and octahedral sites depends on the overall hydrogen concentration. At low H concentration, H prefers octahedral interstitial sites in both hcp Ti and fcc Ti, while at high concentration, H prefers the tetrahedral interstitial sites in the fcc host. This result persists at finite temperature as predicted both by the dilute solution model for the hcp host and the Monte Carlo simulations for the fcc host. For the hcp host with dilute H, the octahedral site is more stable than the tetrahedral site by 76 meV. For the fcc-Ti host, the site occupancy, which is defined as the number of H in a particular type of interstitial site divided by the total number of that type of interstitial site, can be extracted from the Monte Carlo simulations. Figure 6 illustrates the site occupancy as a function of H concentration at 300 and 600 K for the fcc-Ti host. As is evident from Fig. 6, H

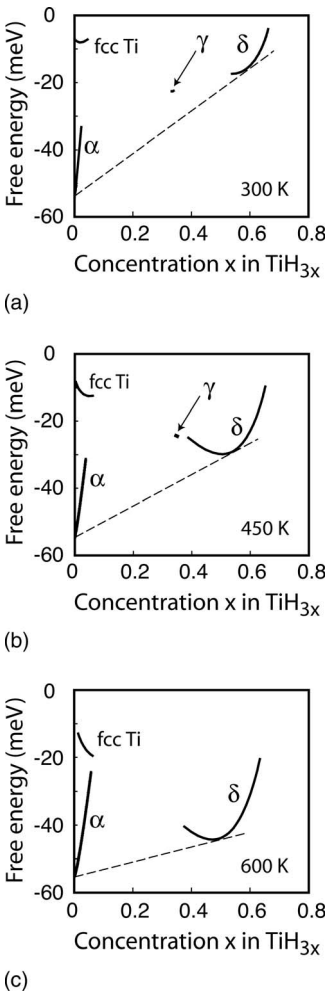

FIG. 5. Free energies of fcc Ti, α-Ti (hcp), γ-TiH, and δ-TiH_2 at (a) 300 K, (b) 450 K, and (c) 600 K.

prefers the octahedral sites at low concentration, while it prefers the tetrahedral sites at high H concentration, although at 600 K some octahedral occupancy also exists in the H-rich δ-TiH_2 phase at hydrogen compositions near the two-phase coexistence boundary.

B. Vibrational degrees of freedom

The analysis of phase stability in the Ti-H system has so far only taken account of configurational degrees of freedom. However, due to the low mass of hydrogen, vibrational degrees of freedom can be important, especially zero-point vibrational energies. To investigate this, we calculated the phonon densities of states of 30 different H-vacancy configurations within the fcc-Ti host along with the phonon density of states for hcp Ti. These were calculated with a force-constant spring model.[38] The force constants were extracted from first-principles GGA calculations (with the VASP code) of the restoring forces due to atomic perturbations within supercells using the FITFC code of the Alloy Theoretic Automated Toolkit.[38,55] For each fcc based configuration, we used a supercell with maximal length between periodic images of 9 Å and extracted spring constants up to an interatomic distance of 4.5 Å. Convergence tests for several hydrogen-vacancy arrangements indicated that these supercell sizes and spring cutoff lengths lead to a numerical error in the zero-point vibrational energies of about 1 meV per formula unit of TiH_{3x}.

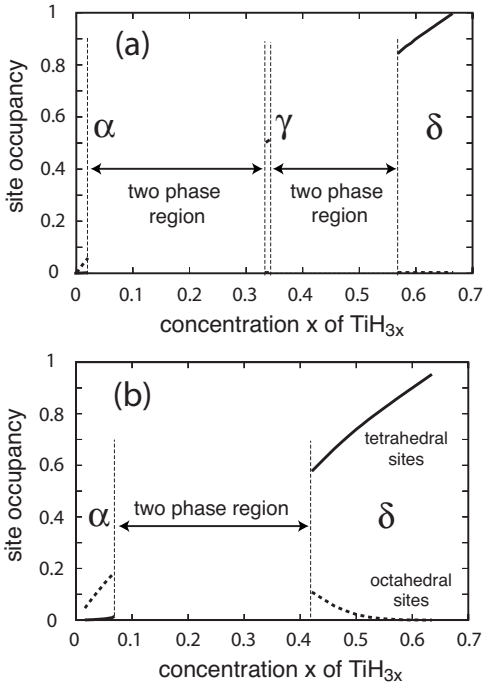

FIG. 6. Hydrogen concentration within tetrahedral (solid lines) and octahedral (dashed lines) sites of the fcc-Ti host at (a) 300 K and (b) 600 K.

Among the 30 configurations for which phonon densities of states were calculated, eight exhibited unstable phonon modes. The formation energies with and without zero-point vibrational energy of the remaining 22 stable H-vacancy configurations are illustrated in Fig. 7. The formation energies are relative to the fcc-Ti and δ-TiH_2 reference states (also with and without zero-point vibrational energies, respectively). Figure 7 clearly shows that zero-point vibrational energy can have a significant effect on the formation energies of some configurations in a hydrogen containing system. In fact, inclusion of zero-point vibrational energy raises the formation energy of γ-TiH by 19 meV, thus making this phase even less stable relative to α-Ti and δ-TiH_2 already at 0 K.

The effect of zero-point vibrational energy on formation energies also differs qualitatively depending on whether hydrogen atoms occupy tetrahedral sites or octahedral sites. Among the 22 configurations of Fig. 7, 15 configurations have exclusive tetrahedral occupancy by hydrogen, three configurations with a hydrogen concentration x less than 1/6 have octahedral-hydrogen occupancy only, while the remaining three configurations, which have relatively high formation energies, have both tetrahedral and octahedral hydrogen (the last configuration is pure fcc without H). We found that zero-point vibrational energy raises the formation energies of most low energy configurations containing tetrahedral sites, while it lowers the formation energy for configurations with octahedral hydrogen. This is presumably due to the larger

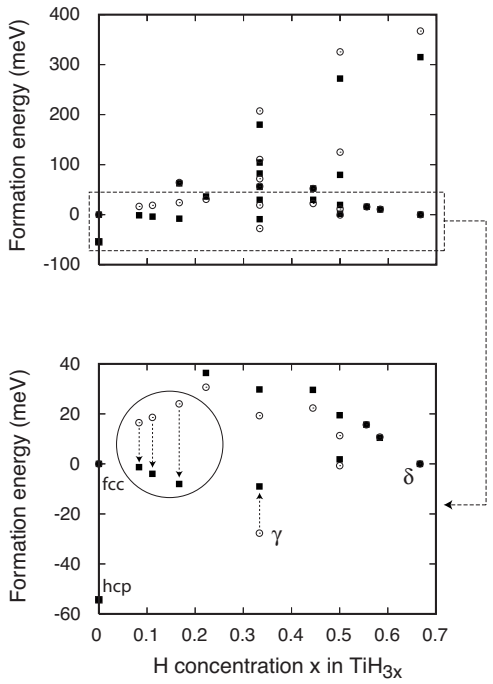

FIG. 7. Formation energies of various configurations of TiH_{3x} with (squares) and without (circles) zero-point vibrational energies. Reference states are fcc Ti and δ-TiH_2. The circled energies correspond to configurations with exclusively octahedral occupancy. All other energies in the enlarged plot (bottom) correspond to configurations with exclusively tetrahedral occupancy.

interatomic distance between H and Ti in the octahedral sites as compared to tetrahedral sites. Larger interatomic distances tend to lead to softer bonds (smaller force constants) and therefore vibrational densities of states corresponding to lower frequencies.[38]

Similar trends were found in hcp Ti. Inclusion of zero-point vibrational energy raised the difference in energy between tetrahedral versus octahedral occupancy by hydrogen (in the dilute limit) from 76 to 146 meV, further destabilizing the tetrahedral site in this dilute regime. These energy differences were calculated in a 36-atom hcp Ti supercell containing one hydrogen atom. The phonon densities of states of an isolated hydrogen atom in hcp Ti were calculated with a force-constant spring model, fit to first-principles GGA calculations of atomic perturbations in the 36-atom unit cell.

We point out that a harmonic spring model for a particular crystal can fail to predict mechanical instabilities if the force constants are too short ranged. Extending force constants to larger distances than used in this work, or using a linear response method to calculate the phonon density of states, may indicate that even more than eight of the 30 H-vacancy configurations considered here are mechanically unstable. In fact, the short-ranged spring model failed to predict the mechanical instability of cubic TiH_2 with respect to a homogeneous tetragonal distortion [see Fig. 2(a)].

C. Cubic to tetragonal phase transformation of TiH_2

We have so far focused on hydrides in the Ti-H system that form as the result of hydrogen ordering over the interstitial sites of fcc Ti. However, in addition to the γ-TiH and δ-TiH_2 hydrides, a third hydride can form, denoted ε-TiH_2, as a result of a structural cubic to tetragonal transformation from cubic δ-TiH_2 around 300 K.[22] A distinction can be made between structural transformations that involve an internal shuffle, in which atoms within a unit cell rearrange at a transition temperature and thereby change the symmetry of the crystal, and structural transformations involving a homogeneous strain of the unit cell. The cubic δ-TiH_2 to tetragonal ε-TiH_2 phase transformation falls into the second category. The first category has been studied extensively in the context of ferroelectric phase transformations using first-principles effective Hamiltonians.[56–59] The second category of structural phase transformations is less well understood from a statistical mechanical point of view.

While the cubic form of TiH_2 is observed experimentally above $\sim$300 K,[22] calculations within density functional theory predict that this phase is mechanically unstable with respect to a tetragonal distortion at 0 K [see Fig. 2(a) and Ref. 52]. Conventional intuition about structural phase transformations is typically based on a Landau interpretation in which temperature dependent free energies are assumed to exist as a function of some order parameter, which, in the case of TiH_2, would be the c/a ratio. As the temperature increases, the shape of the free energy should change in a way that renders the high-temperature phase both mechanically stable and as having the lowest free energy. For TiH_2, this picture implies that vibrational and electronic excitations should make the cubic form of TiH_2 mechanically stable at a finite temperature, as reflected by a free energy curve exhibiting a local minimum around $c/a=1$. Here, we explore the extent with which electronic and harmonic vibrational excitations at finite temperature affect the free energy of TiH_2 as a function of the c/a ratio.

The cubic to tetragonal phase transformation of TiH_2 has been suggested to originate from a Jahn-Teller instability.[60,61] Experiments as well as density functional theory calculations[52,60,61] have demonstrated that the Fermi level of cubic TiH_2 [and ZrH_2 (Refs. 52, 62, and 63)] coincides with a peak in the electronic density of states. A tetragonal distortion of TiH_2 splits this peak,[61] resulting in a minimum in the density of states at the Fermi level and a lowering of the total energy of the crystal. At elevated temperature, however, thermally excited electrons will start occupying the split off empty states above the Fermi level of the tetragonal phase, thereby undoing the energy gain of the Jahn-Teller distortion. We can therefore expect a critical temperature above which the cubic form of TiH_2 should become mechanically stable and have a free energy that is lower than tetragonal TiH_2.

In order to qualitatively investigate the role of thermal electronic excitations on the cubic to tetragonal phase transformation, we calculated the free energy of TiH_2 as a function of the c/a ratio due to electronic excitations by varying the degree of thermal broadening of the electron distribution around the Fermi level using the Fermi smearing feature in VASP calculations with a smearing factor given by $\sigma=k_BT$. Figure 8 illustrates the calculated free energies at various temperatures T. In these calculations, we used a sufficiently dense k-point grid ($24\times24\times24$ mesh for the nonprimitive fcc form of TiH_2) to ensure k-point convergence for each

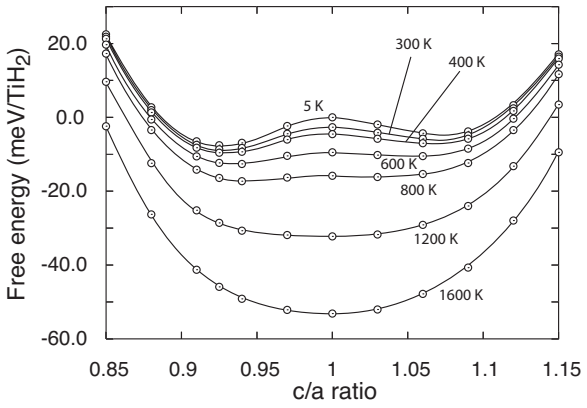

FIG. 8. Free energies of TiH_2 as a function of c/a ratio, calculated with Fermi broadening of the electron distribution at various temperatures.

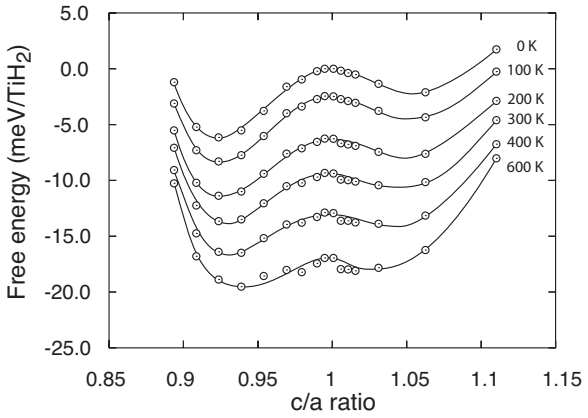

FIG. 9. Constrained free energies of TiH_2 as a function of c/a ratio, calculated within the harmonic approximation using a first-principles parametrized spring model. The free energies at finite temperature are shifted to fit in one plot.

value of σ. Figure 8 clearly shows that the difference in free energy between tetragonal and cubic TiH_2 decreases with increased broadening (due to increased temperature) of the electron distribution around the Fermi level. Furthermore, the c/a ratio corresponding to the minimum free energy gradually approaches 1 as the temperature increases. Nevertheless, the cubic phase remains mechanically unstable with respect to tetragonal distortion up to temperatures in excess of 800 K, which is well above the experimentally measured cubic to tetragonal transition temperature of 300 K. This result suggests that electronic excitations alone cannot account for the experimentally observed cubic to tetragonal phase transformation of TiH_2 at 300 K.[22] Other factors related to vibrational degrees of freedom must therefore also play an important role in this transformation.

The fact that a short-ranged spring model fails to predict mechanical instabilities due to homogeneous strains of cubic TiH_2, as described in Sec. III B, provides us with an opportunity to calculate a constrained free energy as a function of the c/a ratio due to harmonic vibrational degrees of freedom, even for the portions that are mechanically unstable with respect to a homogeneous tetragonal distortion. This is illustrated in Fig. 9 where Eq. (3) is evaluated as a function of the c/a ratio using phonon-dispersion curves calculated within the harmonic approximation with force constants derived from perturbations in supercells having a distance of 11.5 Å between periodic images and spring constants extending to 5.7 Å. Figure 9 shows that the mechanical instability of cubic TiH_2 with respect to a homogeneous (acoustic) strain persists to temperatures above the experimental cubic to tetragonal transition temperature of 300 K. Although the free energies of Fig. 9 are calculated with a first-principles parametrized spring model, they should be viewed as phenomenological free energy curves not unlike Landau free energies expressed as a function of a strain order parameter. Presumably, the free energy curves of Fig. 9, while based on a harmonic spring model that fails to capture the instability of long-wavelength tetragonal distortions of the crystal, accurately account for optical and short-wavelength phonon excitations, which are more easily described with short-range spring constants.

The calculated free energies of Figs. 8 and 9 suggest that a conventional Landau interpretation of the cubic to tetragonal phase transformation, involving free energies that are assumed to have local minima for both the tetragonal and cubic phases as a function of c/a, does not apply to TiH_2. Our results indicate that neither electronic excitations nor short-wavelength harmonic vibrations alone can explain the existence of cubic TiH_2 above 300 K, implying that anharmonic vibrational degrees of freedom must also play an important role in stabilizing the cubic phase at high temperature. A more accurate treatment of the relevant finite temperature excitations that stabilize cubic TiH_2 at finite temperature will require an explicit description of the anharmonic vibrational degrees of freedom with, for example, Monte Carlo simulations applied to an anharmonic strain Hamiltonian that describes the large degree of anharmonicity with respect to long-wavelength tetragonal distortions.

As was noted in Sec. III A 1, the mechanical instability of cubic TiH_2 persists as the hydrogen concentration is reduced [see Figs. 2(b) and 2(c)], although the difference in energy between the stable tetragonal variant and the cubic form of TiH_{2-z} reduces to around 3 meV per TiH_{2-z} formula unit. A rigorous characterization of the thermodynamic properties of the cubic form of TiH_{2-z}, therefore, requires the inclusion of not only configurational degrees of freedom but also anharmonic vibrational degrees of freedom. This could be achieved with an effective Hamiltonian that couples both configurational degrees of freedom with anharmonic strain degrees of freedom. Due to the extra degrees of freedom that are readily excited at low temperature, in addition to configurational degrees of freedom, we can expect an explicit inclusion of strain fluctuations to lead to a further stabilization of the δ-TiH_{2-z} phase and an increase in the off stoichiometry that can be tolerated by δ-TiH_{2-z}. An explicit inclusion of the anharmonic strain fluctuations, while more rigorous, is unlikely to qualitatively alter the results of Sec. III A with respect to the off stoichiometry predicted for δ-TiH_2 or the stability of γ-TiH relative to α-Ti and δ-TiH_2. Nevertheless, such a treatment would enable the prediction of the composition dependence of the δ to ε cubic to tetrag-

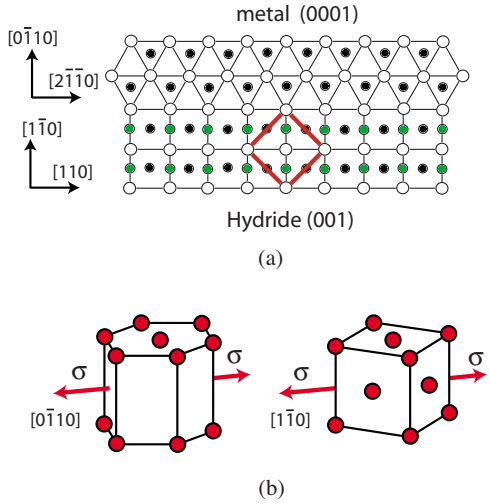

FIG. 10. (Color online) (a) The experimentally observed (Ref. 23) habit plane between α-Ti (hcp) and coherent γ-TiH precipitates. Empty and black circles are Ti atoms of successive (0001) and (001) planes of the hcp and fcc hosts and green circles are tetrahedrally coordinated hydrogen atoms. (b) Schematic illustration of the orientation of the axis of tension relative to the hcp and fcc hosts used to investigate the role of stress on hydride phase stability.

onal transformation temperature and would shed light on the thermodynamic properties of high-temperature phases that are predicted to be mechanically unstable at 0 K.

D. Role of stress and coherency strains

Crack growth in Ti within a hydrogen-rich environment is often accompanied by hydride formation ahead of the crack tip under slow loading conditions.[3] This experimental observation suggests that the Ti hydrides become thermodynamically more favored under a state of tensile stress. Even in the absence of external loads, internal stresses that could alter the relative stability of the various phases competing for stability can arise during solid-state phase transformations due to coherency strains and volumetric changes. In fact, Numakura and Koiwa[23] observed that thin platelike γ-TiH precipitates form coherently within the α-Ti matrix during the early stages of hydride formation. Their TEM analysis elucidated the crystallographic relationship between γ-TiH and the α-Ti matrix, showing that the coherent interface consists of a prismatic $\{0\bar{1}10\}$ plane of the hcp Ti matrix on one side and the $\{1\bar{1}0\}$ plane of γ-TiH precipitate on the other. Figure 10(a) schematically illustrates this coherent interface between α-Ti and γ-TiH, reproduced from Numakura and Koiwa.[23]

When a thin, extended γ-TiH plate forms coherently within the α-Ti matrix, its lattice parameters parallel to the coherent interface will be constrained by those of the matrix phase, thereby leading to a state of internal stress within the precipitate. To ensure coherency between α-Ti and γ-TiH along the interface illustrated in Fig. 10(a), d_{220} must equal $d_{2\bar{1}\bar{1}0}$ and d_{002} must equal d_{0002}, where d_{hkl} and d_{hklm} are interplanar spacings of atomic planes in the precipitate and matrix, respectively. The lattice parameter of γ-TiH perpendicular to the coherent interface, i.e., the $[1\bar{1}0]$ direction, can potentially relax. The degree to which this lattice parameter relaxes depends on the overall geometry of the specimen as well as the elastic stiffness of the matrix phase. Due to a volumetric increase upon hydride formation, it is likely that the precipitate will experience some degree of compressive stress perpendicular to the interface.

A phase diagram can be constructed displaying the relative stability between α-Ti, γ-TiH, and δ-TiH_2 as a function of stress. Figure 11 illustrates two such phase diagrams showing relative stability as a function of μ_H and a uniaxial stress σ calculated by minimizing the grand force potential Φ introduced in Sec. II [Eq. (5)]. These phase diagrams were calculated at 0 K, where the entropy is zero and only stoichiometric compounds exist. Hence, the internal energy E appearing in Eq. (5) is then simply equal to the first-principles energy (GGA) of either α-Ti, γ-TiH, or δ-TiH_2 as a function of the stress σ. In Eq. (5), the strain ε is also a function of the stress σ and this dependence is particular to each phase. Practically determining the potential Φ at 0 K can proceed by calculating E versus the strain ε and then extracting the stress σ by taking the derivative of E with respect to ε and dividing by V_o.

The phase diagrams in Fig. 11 correspond to two particular states of lateral strain perpendicular to the axis of tension. The axis of tension is along the $[0\bar{1}10]$ direction of the hcp crystal and the $[1\bar{1}0]$ direction of the Ti fcc sublattice of γ-TiH or δ-TiH_2 [Fig. 10(b)]. If hydrides form coherently within the α-Ti matrix according to the crystallographic orientations reported by Numakura and Kaiwa,[23] the tension along the $[0\bar{1}10]$ axis of hcp Ti would coincide with tension

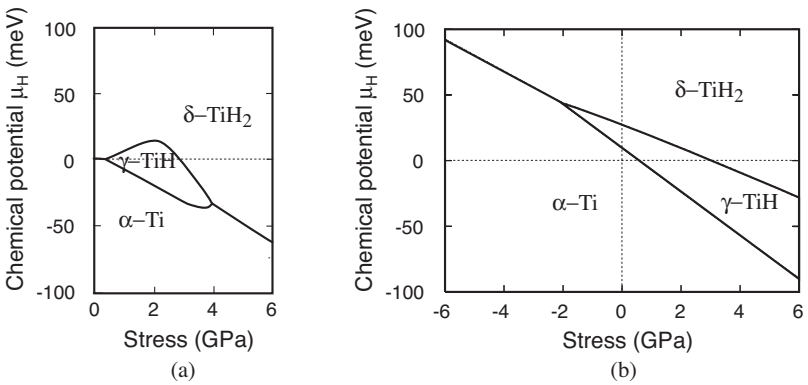

FIG. 11. 0 K phase diagrams as a function of hydrogen chemical potential and stress (see Fig. 10 for the orientation of the applied stress relative to the various crystals). (a) Phase diagram in the absence of coherency strains (i.e., equilibrium lattice parameters perpendicular to the axis of tension). (b) Phase diagram accounting for coherency strains that exist across the habit plane of Fig. 10(b).

along the $[1\bar{1}0]$ direction of the fcc sublattice of γ and δ hydrides and would be perpendicular to the coherent interface. The phase diagram of Fig. 11(a) was calculated for crystals in the absence of coherency strains. The phase diagram of Fig. 11(b) was calculated by fixing the hydride lattice parameters perpendicular to the axis of tension to coincide with those of hcp Ti in the $\{0\bar{1}10\}$ plane. Figure 11(b) therefore corresponds to a phase diagram describing coherent hydride phase stability. The phase diagrams neglect zero-point energies and therefore only provide general trends as to how hydride phase stability evolves with increasing stress.

Figure 11(a) shows that at low hydrogen chemical potential, α-Ti is stable, while at high chemical potential, δ-TiH_2 is stable. The reference state of the hydrogen chemical potential is arbitrarily set to the value corresponding to the transition between α-Ti and δ-TiH_2 at zero stress. As already mentioned in Sec. III A 3, bulk γ-TiH is not stable at zero pressure and therefore does not appear in the phase diagram of Fig. 11(a) at $\sigma=0$. As stress is imposed, however, γ-TiH becomes stable within a limited range of stress and hydrogen chemical potential. The phase diagram of Fig. 11(a) also illustrates that stress along the $[0\bar{1}10]$ direction of α-Ti and the $[1\bar{1}0]$ of the δ-TiH_2 favors hydride formation as manifested by the negative slope of the phase boundary between α-Ti and δ-TiH_2: As the tensile stress σ is increased, the transition from α-Ti to δ-TiH_2 occurs at a lower hydrogen chemical potential. This result is consistent with experimental observations of hydride formation ahead of a crack tip.[3]

The stability of the γ-TiH phase relative to α-Ti and δ-TiH_2 is significantly enhanced when a strain perpendicular to the axis of tension is imposed on the hydrides to enable the formation of coherent interfaces with the α-Ti matrix along the $(0\bar{1}10)$ habit plane, as illustrated in Fig. 10(b). When coherency strains are imposed, γ-TiH even becomes stable for compressive stresses within a limited chemical potential range. For a coherent γ-TiH hydride, the chemical potential interval in which γ-TiH is stable increases with increasing tensile stress perpendicular to the $(0\bar{1}10)$ habit plane.

IV. CONCLUSION

A first-principles investigation of the thermodynamic properties of the Ti-H system has revealed the importance of configurational and vibrational degrees of freedom in determining hydride phase stability. Configurational excitations are important in δ-TiH_{2-z} as this phase can tolerate large vacancy concentrations, while they do not contribute significantly to the free energy of the γ-TiH phase, which remains a stoichiometric compound at finite temperature. The inclusion of zero-point vibrational energy penalizes tetrahedral site occupancy more than octahedral site occupancy and increases the degree with which γ-TiH is unstable relative to α-Ti and δ-TiH_2. This favoring of octahedral sites over tetrahedral sites by vibrational degrees of freedom is likely a general trend in all metallic hydrides. An analysis of relative stability under anisotropic stress states shows that hydrides of the Ti-H system are thermodynamically favored under tensile stress. When the hydrides are subjected to coherency strains, γ-TiH is predicted to be stable at zero stress as well as under compressive stresses. The predicted mechanical instability of cubic δ-TiH_2 with respect to a homogeneous tetragonal distortion to ε-TiH_2 raises fundamental questions about the relevant excitations that stabilize cubic TiH_2 above 300 K and suggests the importance of anharmonic strain fluctuations in determining the thermodynamic properties of this phase.

[1] L. Schlapbach and A. Zuttel, Nature (London) **414**, 353 (2001).
[2] H. K. Birnbaum, M. L. Grossbeck, and M. Amano, J. Less-Common Met. **49**, 357 (1976).
[3] D. S. Shih, I. M. Robertson, and H. K. Birnbaum, Acta Metall. **36**, 111 (1988).
[4] S. Takano and T. Suzuki, Acta Metall. **22**, 265 (1974).
[5] J. P. Hirth and J. R. Rice, Metall. Trans. A **11**, 1501 (1980).
[6] R. A. Oriani and P. H. Josephic, Acta Metall. **22**, 1065 (1974).
[7] A. Van der Ven and G. Ceder, Acta Mater. **52**, 1223 (2004).
[8] A. Van der Ven and G. Ceder, Phys. Rev. B **67**, 060101(R) (2003).
[9] C. D. Beachem, Metall. Trans. **3**, 437 (1972).
[10] H. K. Birnbaum and P. Sofronis, Mater. Sci. Eng., A **176**, 191 (1994).
[11] G. Lu, Q. Zhang, N. Kioussis, and E. Kaxiras, Phys. Rev. Lett. **87**, 095501 (2001).
[12] C. Q. Chen, S. X. Li, and K. Lu, Acta Mater. **51**, 931 (2003).
[13] C. Q. Chen, S. X. Li, H. Zheng, L. B. Wang, and K. Lu, Acta Mater. **52**, 3697 (2004).
[14] D. F. Teter, I. M. Robertson, and H. K. Birnbaum, Acta Mater. **49**, 4313 (2001).
[15] G. H. Kim, C. H. Chun, S. G. Lee, and J. Y. Lee, Acta Metall. Mater. **42**, 3157 (1994).
[16] N. Michel *et al.*, J. Alloys Compd. **330**, 280 (2002).
[17] H. H. Lee, K. Y. Lee, and J. Y. Lee, J. Alloys Compd. **239**, 63 (1996).
[18] T. Schober and W. Schafer, J. Less-Common Met. **74**, 23 (1980).
[19] B. Bogdanovic and M. Schwickardi, J. Alloys Compd. **253**, 1 (1997).
[20] J. E. Bailey, Acta Metall. **11**, 267 (1963).
[21] G. J. C. Carpenter, Acta Metall. **26**, 1225 (1978).
[22] H. L. Yakel, Acta Crystallogr. **11**, 46 (1958).
[23] H. Numakura and M. Koiwa, Acta Metall. **32**, 1799 (1984).
[24] H. Numakura, M. Koiwa, H. Asano, and F. Izumi, Acta Metall. **36**, 2267 (1988).
[25] H. Numakura, M. Koiwa, H. Asano, H. Murata, and F. Izumi, Scr. Metall. **20**, 213 (1986).
[26] D. deFontaine, Solid State Phys., Adv. Res. Appl. **47**, 33 (1994).
[27] V. Ozolins, C. Wolverton, and A. Zunger, Phys. Rev. B **57**, 6427 (1998).
[28] A. Seko, K. Yuge, F. Oba, A. Kuwabara, I. Tanaka, and T. Yamamoto, Phys. Rev. B **73**, 094116 (2006).

[29] A. Van De Walle and G. Ceder, J. Phase Equilib. **23**, 348 (2002).
[30] A. Van Der Ven, M. K. Aydinol, G. Ceder, G. Kresse, and J. Hafner, Phys. Rev. B **58**, 2975 (1998).
[31] A. Van Der Ven and G. Ceder, Phys. Rev. B **71**, 054102 (2005).
[32] C. Wolverton, V. Ozolins, and A. Zunger, Phys. Rev. B **57**, 4332 (1998).
[33] M. E. A. Y. De Dompablo, A. Van Der Ven, and G. Ceder, Phys. Rev. B **66**, 064112 (2002).
[34] H. R. Tang, A. Van Der Ven, and B. L. Trout, Phys. Rev. B **70**, 045420 (2004).
[35] D. J. Siegel, C. Wolverton, and V. Ozolins, Phys. Rev. B **75**, 014101 (2007).
[36] J. M. Sanchez, F. Ducastelle, and D. Gratias, Physica A **128**, 334 (1984).
[37] G. Ceder, Comput. Mater. Sci. **1**, 144 (1993).
[38] A. Van De Walle and G. Ceder, Rev. Mod. Phys. **74**, 11 (2002).
[39] S. Baroni, S. de Gironcoli, A. Dal Corso, and P. Giannozzi, Rev. Mod. Phys. **73**, 515 (2001).
[40] S. Wei and M. Y. Chou, Phys. Rev. Lett. **69**, 2799 (1992).
[41] A. Zunger, in *Statics And Dynamics Of Alloy Phase Transformations*, NATO ASI Series, Vol. 319, edited by P. E. A. Turchi and A. Gonis (Plenum, New York), pp. 361.
[42] R. R. Picard and R. D. Cook, J. Am. Stat. Assoc. **79**, 575 (1984).
[43] J. Shao, J. Am. Stat. Assoc. **88**, 486 (1993).
[44] G. L. W. Hart, V. Blum, M. J. Walorski, and A. Zunger, Nat. Mater. **4**, 391 (2005).
[45] G. Kresse and J. Furthmuller, Phys. Rev. B **54**, 11169 (1996).
[46] G. Kresse and J. Furthmuller, Comput. Mater. Sci. **6**, 15 (1996).
[47] P. E. Blochl, Phys. Rev. B **50**, 17953 (1994).
[48] G. Kresse and D. Joubert, Phys. Rev. B **59**, 1758 (1999).
[49] H. J. Monkhorst and J. D. Pack, Phys. Rev. B **13**, 5188 (1976).
[50] M. Methfessel and A. T. Paxton, Phys. Rev. B **40**, 3616 (1989).
[51] C. Kittel, *Introduction to Solid State Physics*, 6th ed. (Wiley, New York, 1986).
[52] W. Wolf and P. Herzig, J. Phys.: Condens. Matter **12**, 4535 (2000).
[53] G. J. Ackland, Phys. Rev. Lett. **80**, 2233 (1998).
[54] A. Van De Walle and M. Asta, Modell. Simul. Mater. Sci. Eng. **10**, 521 (2002).
[55] A. Van De Walle, M. Asta, and G. Ceder, CALPHAD: Comput. Coupling Phase Diagrams Thermochem. **26**, 539 (2002).
[56] K. M. Rabe and U. V. Waghmare, Phys. Rev. B **52**, 13236 (1995).
[57] U. V. Waghmare and K. M. Rabe, Phys. Rev. B **55**, 6161 (1997).
[58] W. Zhong, D. Vanderbilt, and K. M. Rabe, Phys. Rev. B **52**, 6301 (1995).
[59] W. Zhong, D. Vanderbilt, and K. M. Rabe, Phys. Rev. Lett. **73**, 1861 (1994).
[60] F. Ducastelle, R. Candron, and P. Costa, J. Phys. (Paris) **31**, 57 (1970).
[61] M. Gupta, Solid State Commun. **29**, 47 (1979).
[62] R. C. Bowman, E. L. Venturini, B. D. Craft, A. Attalla, and D. B. Sullenger, Phys. Rev. B **27**, 1474 (1983).
[63] M. Gupta, Phys. Rev. B **25**, 1027 (1982).